RESEARCH ARTICLE

Key Points:
- SMOS ice thickness data have been first assimilated using a local SEIK filter
- SMOS ice thickness assimilation leads to substantially improved thickness

Assimilating SMOS sea ice thickness into a coupled ice-ocean model using a local SEIK filter

Qinghua Yang[1,2], Svetlana N. Losa[2], Martin Losch[2], Xiangshan Tian-Kunze[3], Lars Nerger[2], Jiping Liu[4], Lars Kaleschke[3], and Zhanhai Zhang[5]

[1]Polar Environmental Research and Forecasting Division, National Marine Environmental Forecasting Center, Beijing, China, [2]Alfred Wegener Institute, Helmholtz Centre for Polar and Marine Research, Bremerhaven, Germany, [3]Institute of Oceanography, University of Hamburg, Hamburg, Germany, [4]Department of Atmospheric and Environmental Sciences, University at Albany, State University of New York, Albany, New York, USA, [5]Key Laboratory for Polar Science of the State Oceanic Administration, Polar Research Institute of China, Shanghai, China

Abstract The impact of assimilating sea ice thickness data derived from ESA's Soil Moisture and Ocean Salinity (SMOS) satellite together with Special Sensor Microwave Imager/Sounder (SSMIS) sea ice concentration data of the National Snow and Ice Data Center (NSIDC) in a coupled sea ice-ocean model is examined. A period of 3 months from 1 November 2011 to 31 January 2012 is selected to assess the forecast skill of the assimilation system. The 24 h forecasts and longer forecasts are based on the Massachusetts Institute of Technology general circulation model (MITgcm), and the assimilation is performed by a localized Singular Evolutive Interpolated Kalman (LSEIK) filter. For comparison, the assimilation is repeated only with the SSMIS sea ice concentrations. By running two different assimilation experiments, and comparing with the unassimilated model, independent satellite-derived data, and in situ observation, it is shown that the SMOS ice thickness assimilation leads to improved thickness forecasts. With SMOS thickness data, the sea ice concentration forecasts also agree better with observations, although this improvement is smaller.

1. Introduction

The extent and thickness of the Arctic sea ice cover is in a state of rapid decline [*Kwok and Rothrock*, 2009; *Stroeve et al.*, 2012]. On 16 September 2012, the sea ice extent dropped to 3.41 million km^2, creating a new record summer minimum. This retreat is one of the most visible signs, almost iconographic, of global climate change. Large effects on the climate system are associated with a changing ice cover. For example, the lower surface albedo of open water compared to sea ice has a profound effect on the Arctic surface heat budget. Apart from its relevance to local and global climate, sea ice, or rather its absence is an important factor for shipping and marine operations. Accurate sea ice real-time forecasting has already become an urgent need [*Eicken*, 2013]. Still there are, however, large uncertainties in the modeled Arctic sea ice thickness and volume [*Schweiger et al.*, 2011]. To reduce uncertainties in the sea ice forecast, it is essential to improve the initial conditions of the forecast. The obvious way to improvement involves available observations with advanced data assimilation techniques [*Lisæter et al.*, 2003].

Sea ice concentration has been successfully observed by satellite-based passive microwave instruments for over 30 years. Several studies explored assimilating sea ice concentration observations into coupled ice-ocean models. For example, *Lisæter et al.* [2003] used an ensemble Kalman filter (EnKF) to assimilate Special Sensor Microwave/Imager (SSM/I) sea ice concentration; *Lindsay and Zhang* [2006] employed a nudging scheme to assimilate monthly averaged ice concentration; *Stark et al.* [2008] used an optimal interpolation method to assimilate the SSM/I concentration and sea ice drift data; *Tietsche et al.* [2013] assimilated ice concentration observations with a simple Newtonian relaxation scheme and updated the sea ice thickness analysis using a proportional dependence between concentration and mean thickness in a coupled climate model. Previous studies demonstrated that the assimilation of observed ice concentration in sea ice-ocean models improves the simulated concentration, but most of their improvement in ice thickness was small and not significant. Recently, *Yang et al.* [2014] assimilated summer ice concentration observations with a localized ensemble-based Singular Evolutive Interpolated Kalman (LSEIK) filter. Their results showed that the covariance between ice concentration and thickness can improve summer sea ice thickness.

Observing sea ice thickness from space is a challenge [*Kwok and Sulsky*, 2010; *Tian-Kunze et al.*, 2014]. Although the altimeter observations from ICESat (2003–2009) and CryoSat-2 (since 2011) can detect thick ice, these observations typically have a temporal resolution of 1 month and a spatial resolution of 100 km. Thus, these data are not suited for forecasting systems that require daily updates and high spatial resolution. Due to the sparsity of gridded sea ice thickness observations, there are very few assimilation studies with ice thickness. For example, *Lisæter et al.* [2007] examined the potential for ice thickness assimilation in coupled sea ice-ocean models by assimilating synthetic CryoSat data with an EnKF. Their experiments illustrated that ice thickness assimilation can have a strong impact on the solution fields.

Data of the Soil Moisture and Ocean Salinity (SMOS) mission of the European Space Agency (ESA), launched in November 2009 [*Mecklenburg et al.*, 2012], have been used to derive sea ice thickness [*Kaleschke et al.*, 2012; *Huntemann et al.*, 2014]. Compared to IceSat and CryoSat-2 data, SMOS-derived ice thickness is more accurate in the thin ice regime, but observations of thick ice are not reliable [*Kaleschke et al.*, 2012; *Tian-Kunze et al.*, 2014]. An operational SMOS-based sea ice thickness product with data starting in 2010 has recently been released by the University of Hamburg [*Tian-Kunze et al.*, 2014]. This data set provides error estimates on a daily basis. Thus, this data provide us with an opportunity to assimilate the daily near real-time basin-scale sea ice thickness observation.

In this study, we focus on the autumn-winter seasonal transition period, and the SEIK algorithm applied by *Yang et al.* [2014] is extended here to assimilate not only SSMIS concentration, but also SMOS sea ice thickness into a sea ice-ocean model over a freezeup period of 3 months. The effectiveness of the assimilation system is analyzed by comparing to the assimilated ice concentration and thickness data and to a different satellite-derived ice concentration product. We evaluate 24 h forecasts, but also longer forecasts of 1, 2, and 3 months. In addition, the influence of the assimilation is assessed with independent in situ ice thickness data.

The paper is organized as follows: in section 2, the sea ice-ocean model and the atmospheric forcing are presented. The LSEIK filter and the setup of the data assimilation experiments are introduced in section 3 and the sea ice observational data in section 4. Section 5 describes the approximation of model and data error statistics used in this study. Section 6 discusses the performance of the assimilation runs compared to a model run without assimilation, with a focus on the improvement due to the SMOS assimilation. The study is summarized in section 7.

2. Numerical Sea Ice-Ocean Model and Atmospheric Forcing

The model and atmospheric forcing used in this study is exactly the same as in *Yang et al.* [2014]. The Massachusetts Institute of Technology general circulation model (MITgcm) [*Marshall et al.*, 1997] has a sea ice module with state of the art dynamics [*Losch et al.*, 2010] based on *Zhang and Hibler* [1997]. It has been used in Arctic regional studies at varying resolution [*Losch et al.*, 2010; *Nguyen et al.*, 2011, 2012]. A regional MITgcm configuration [*Losch et al.*, 2010; *Nguyen et al.*, 2011] is used in our Arctic modeling and forecasting experiments. The modeling domain covers a limited Arctic area with open boundaries at ≈55°N in both the Atlantic and Pacific sectors. A global configuration [*Menemenlis et al.*, 2008] is used to provide monthly boundary conditions of potential temperature, salinity, current, and sea-surface elevation. The grid covering the Arctic domain is locally orthogonal and has a variable horizontal resolution with an average spacing of 18 km. The sea ice and ocean equations are solved on the same horizontal mesh. The vertical resolution is highest in the upper ocean, with 28 vertical levels in the top 1000 m. Bathymetry is derived from the U.S. National Geophysical Data Center (NGDC) 2 min global relief data set (ETOPO2) [*Smith and Sandwell*, 1997]. The monthly mean river runoff is based on the Arctic Runoff Data Base (ARDB) as prepared by P. Winsor [*Nguyen et al.*, 2011].

The model is forced here with atmospheric field of the analysis (Climate Data Assimilation System; JCDAS) from the Japan Meteorological Agency (JMA). This analysis started in January 2005, and the JCDAS is consistent with the data assimilation applied in Japanese 25 year Reanalysis (JRA25) [*Onogi et al.*, 2007] that has been used in spin-up simulations [*Nguyen et al.*, 2011].

3. Data Assimilation

The sea ice observations are assimilated with a SEIK filter [*Pham*, 2001] combined with a localized state correction (LSEIK). The SEIK filter is an ensemble-based Kalman filter method. It is implemented in the Parallel

Data Assimilation Framework (PDAF, http://pdaf.awi.de) [*Nerger and Hiller*, 2013]. In the filter, the sea ice observations are combined with the model state estimate taking into account the assumed model errors as well as the error in the model state estimate. The model state error is estimated from the spread of an ensemble of model states. The SEIK filter has already been used to assimilate sea ice motion in a stand-alone sea ice model [*Rollenhagen et al.*, 2009] and for sea-ice concentration assimilation [*Yang et al.*, 2014]. The filter algorithm can be divided into four phases: initialization, forecast, analysis, and ensemble transformation, which are described below. For a detailed derivation of the LSEIK filter from the global SEIK filter, see *Nerger et al.* [2006].

The initial ensemble provides an estimate of the initial model state and its uncertainty before the assimilation of sea ice observations. The initial model state uncertainties are estimated from the variability of the prescribed model dynamics under variable atmospheric forcing [see *Losa et al.*, 2012, 2014]. For simplicity, the initial state error covariance matrix of sea ice concentration and thickness is estimated based on a model integration over the period of 1 October 2011 to 31 December 2011 that is initialized by an optimized ocean-sea ice spin-up run [*Nguyen et al.*, 2011]. The information from this partly overlapping period is only used in creating the initial state error covariance. In an operational application, one would use a similar sampling period from the previous model year, or maybe even averaged over many previous model years. One time slice per day is stored, resulting in 92 state vectors that describe the model variability and the observed dynamics. Using second-order exact sampling [*Pham*, 2001], the leading EOFs of the model variability sampled by the daily outputs are used to generate an ensemble of 15 initial model states of ice concentration and thickness. This ensemble dynamically evolves in time and represents the full state error covariance matrix, hence variances as well as all covariances between different locations and model fields.

The filter is split into two alternating phases: the forecast phase and the analysis step. In the forecast phase, all ensemble states are evolved by the MITgcm model for 24 h taking into account the atmospheric forcing. The analysis step incorporates the observational information into the model state by computing a state correction. For this, the SEIK filter estimates the uncertainty of the state estimate from the ensemble covariance matrix. The analysis correction of the state is then computed as a linear combination of the forecast ensemble anomalies of the mean state with a coefficient matrix computed from the difference between the model state estimate and the observations, weighted by the observation error covariance matrix and the forecast state error covariance matrix. The analysis step of the Kalman filter also updates the state error covariance matrix, which is estimated by the state ensemble. For this, the forecast ensemble of model states is transformed, so that it represents the state error covariance matrix after the analysis correction. In the analysis step, a domain localization following *Nerger et al.* [2006] is applied where each single water column of the model grid is corrected by assimilating observations only within a specified radius of influence. The localization in the analysis step uses a small cutoff distance of seven grid points (~126 km) in both zonal and meridional direction. As there is no satellite data near the North Pole, a spatially variable localization radius is applied in this area. This radius is gradually increased from eight grid points (~144 km) at the 86°N circle to 29 grid points (~232 km) in the North Pole. With this approach, the observed information from the region south of 86°N is properly extrapolated toward the Pole. Within the cutoff distance, the observations are weighted according to their distance from the grid point inquisition [see *Janjić et al.*, 2011] by a fifth-order polynomial function that mimics a Gaussian distribution [*Gaspari and Cohn*, 1999].

The analysis step performs a statistical update of the state estimate under the assumption of Gaussian errors. The statistical nature of the update does not have a constraint to limit concentrations between 0 and 1.0 so that small negative and unrealistically high values of the ice concentration can occur, in particular, at locations with small forecast concentration and no sea-ice concentration observation. A similar effect can occur for sea-ice thickness. The negative values are set to zero, while concentrations exceeding 1.0 are replaced by 1.0. Unreasonable ice thicknesses are corrected by applying an ice concentration-dependent ice thickness. If the ice thickness is positive while the concentration indicates that there is no ice, the thickness is reset to zero. In contrast, zero ice thickness in the presence of nonzero ice concentration is set to a new ice thickness of 2 m times ice concentration [*Tietsche et al.*, 2013]. The sea surface temperature is not modified directly by the assimilation, but their updates are implicitly provided in the presence of sea ice by the model assumption of thermodynamic equilibrium between sea ice and the ocean surface water layer.

The forecast skill of the system in the transition from autumn to winter is evaluated by two experiments over 1 November 2011 to 31 January 2012. This period is chosen because the SMOS data are limited to the

cold season [*Tian-Kunze et al.*, 2014]. The experiments only differ in the observation data that are assimilated:

1. LSEIK-1: forecasts with sea ice concentration data assimilated at 00:00. This experiment has the same configuration as in the ice concentration assimilation experiment by *Yang et al.* [2014].
2. LSEIK-2: forecasts after assimilating sea ice concentration data and ice thickness data at 00:00.

Note that as in *Yang et al.* [2014], the state vector of the assimilation system consists of sea ice concentration and thickness and has a length of 152,694 (= number of "wet" surface grid points times 2 fields). Only observations of sea ice concentration are assimilated in LSEIK-1, so that the ice thickness is modified only through the forecast state error covariance between ice concentration and thickness. In LSEIK-2, both sea ice concentration and thickness observations are assimilated and the concentration of the analysis is a consequence of both concentration observation and by means of the background error covariance also of observed thickness. Vice versa, the ice thickness in LSEIK-2 is determined by both ice thickness and concentration observations.

4. Sea Ice Data

In this study, observations of both sea ice concentration and sea ice thickness are assimilated. Observations of remotely sensed sea ice concentrations and independent ice thickness data are utilized to validate the assimilation performance.

The ice concentration observations assimilated in both experiments are derived from DMSP F-17 SSMIS passive microwave data, processed by the NSIDC with the NASA team algorithm [*Cavalieri et al.*, 2012], and interpolated to the model grid. The performance of the assimilation is evaluated using near real-time sea ice concentration data from the European Meteorological Satellite Agency (EUMETSAT) Ocean and Sea Ice Satellite Application Facility (OSISAF) [*Eastwood et al.*, 2011]. More specifically, we use the final product of daily fields provided on a 10 km polar stereographic grid. Note that the OSISAF concentration product, at least for the period in question, is derived from a different satellite and sensor (DMSP F-15 SSM/I) with a different algorithm than the NSIDC data. This makes the OSISAF data an independent data set.

Daily averaged sea ice thickness derived from SMOS brightness temperatures is assimilated in the LSEIK-2 forecasting experiment. The SMOS-derived sea ice thickness has been retrieved with an algorithm that is based on a sea ice thermodynamic model and a three-layer radiative transfer model [*Kaleschke et al.*, 2010, 2012], which explicitly takes variations of ice temperature and ice salinity into account [*Tian-Kunze et al.*, 2014]. In this retrieval, a statistical thickness distribution function derived from high-resolution ice thickness measurements has been implemented to correct the underestimation of ice thicknesses caused by the plane ice layer assumption [*Tian-Kunze et al.*, 2014]. The sea ice thickness data have a horizontal grid resolution of 12.5 km, and are interpolated onto the MITgcm model grid (about 18 km resolution). The maximum retrievable SMOS ice thickness varies from a few centimeters to about 1 m depending on the ice temperature and ice salinity. This range doubles when we consider the heterogeneity of ice thicknesses within one SMOS footprint [*Tian-Kunze et al.*, 2014].

A first estimation of SMOS-retrieved ice thickness uncertainty has been given in the released SMOS ice thickness data set. There are several factors that cause the uncertainties in the SMOS ice thickness retrieval: the uncertainty of SMOS brightness temperature measurements, uncertainties in the auxiliary data sets used in the retrieval, and the assumptions made in the retrieval algorithm. Standard deviations of the main parameters like SMOS brightness temperature, ice temperature, and ice salinity were considered for the uncertainty estimation. However, the different error factors are not independent, because they are functions of ice thickness. In the present SMOS data set, each error is estimated by keeping the other parameters constant. The total uncertainty given in the data set is the sum of these errors. Errors caused by the assumptions about fluxes and snow thickness have not yet been included. The SMOS ice thickness uncertainty varies from a few centimeters to up to 1 m for thin ice. In the thick ice range, it is not possible to estimate either the ice thickness or the ice thickness uncertainty using SMOS data. In this case, a constant value of 5 m is given for the uncertainty. Furthermore, SMOS ice thickness uncertainties are not Gaussian distributed, i.e., asymmetric with higher uncertainties with increasing ice thickness. In addition to the uncertainties, SMOS-derived sea ice thickness has systematic errors caused by the 100% ice coverage assumption made
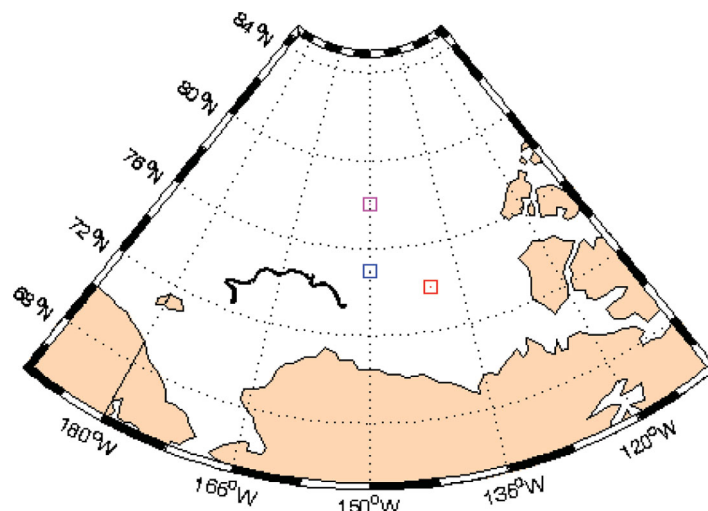
Figure 1. Locations of sea ice thickness observations and buoy trajectory from 1 November 2011 to 31 January 2012. BGEP_2011a (blue square; 74°59.816′N, 149°58.149′W), BGEP_2011b (magenta square; 78°0.395′N, 149°58.462′W), BGEP_2011d (red square; 73°59.649′N, 139°59.043′W), and IMB_2011K (black line).

in the retrieval. *Tian-Kunze et al.* [2014] have investigated the possible underestimation of ice thickness due to this assumption and have found that the bias caused by this assumption increases exponentially with decreasing ice concentration. However, this effect has not yet been corrected in the released SMOS ice thickness data set. In this study, only thicknesses below 1.0 m are assimilated and the provided sea ice thickness uncertainties are used for the error estimation in the assimilation.

To further assess our simulated ice thickness results, independent in situ ice thickness data are used: Sea ice draft from Beaufort Gyre Experiment Program (BGEP) Upward Looking Sonar (ULS) moorings located in the Beaufort Sea over the period of 1 November 2011 to 31 January 2012 (BGEP_2011a, BGEP_2011b, BGEP_2011d; Figure 1) [*Melling et al.*, 1995]; and sea ice thickness data obtained from an autonomous ice mass balance buoys (IMB) [*Perovich et al.*, 2009]. Two acoustic rangefinders on the IMB monitor the position of the ice bottom and the snow and ice surface, which allows to estimate the sea ice thickness. The accuracy of both sounders is 5 mm [*Richter-Menge et al.*, 2006]. In our study period, the IMB_2011K is the only buoy with available data; its trajectory during the study period is shown in Figure 1. The error of ULS measurements of ice draft is estimated as 0.1 m [*Melling et al.*, 1995]. Drafts are converted to thickness by multiplying with a factor of 1.1, which is approximately the ratio of mean seawater density of 1024 kg/m^3 and sea ice density of 910 kg/m^3 [*Nguyen et al.*, 2011].

5. Approximation of Model and Data Error Statistics

The performance of any data assimilative system crucially depends on assumed model and data error statistics and how the statistics evolve in time. Practical applications of data assimilation, however, suffer from the lack of information about model and data error statistics. As a result, terms as "standard deviation of data errors," "data uncertainties," "data errors correlation," usually used in a formal description of DA algorithms, cannot be used in their strict sense. Indeed, they are linked with model uncertainties and the DA algorithm itself [*Kivman et al.*, 2001]. When discussing the statistical properties of data errors used in the filter, we think of them in that conditional context [*Losa et al.*, 2012].

Thus, the uncertainty in the observed sea ice concentrations is on average around 10% [*Tonboe and Nielsen*, 2010]. There is, however, an additional source of the errors because of model representativeness. Moreover, when approximating the sea ice concentration data errors σ_{SIC}, one has to also account for the aforementioned conditional properties of error statistics.

The prior model error statistics were approximated with the initial ensemble of model states generated as described above. In the filter analysis steps, the model error covariances are corrected based on the observational information. The updated ensemble further evolves in time according to the model equations. To account for additional uncertainties in the external forcing, the forecast error statistics are inflated with the so-called "forgetting factor" [*Pham*, 2001] (0.97 in this study).

A series of sensitivity experiments with different prior error statistics have been carried out in order to calibrate the system. We have tested several values of σ_{SIC}, localization radius, and inflation of the forecast error statistics. The assumption on σ_{SIC} = 30% gave the best forecast agreement with observations [*Yang et al.*, 2014].

Table 1. Two-Sample *t* Test (*t* Test2) Results of Sea Ice Concentration and Thickness RMSE[a]

	Statistics	*t* Test2	*p* Value	Degree of Freedom
1	LSEIK-1 versus MITgcm	1-1-0	0.00-0.00-0.07	182
2	LSEIK-2 versus MITgcm	1-1-1	0.00-0.00-0.00	182
3	Forecast initialized on 1 Nov 2011 versus MITgcm	1-1-1	0.00-0.00-0.00	182
4	Forecast initialized on 1 Dec 2011 versus MITgcm	1-1-1	0.00-0.00-0.00	122
5	Forecast initialized on 1 Jan 2012 versus MITgcm	1-1-1	0.00-0.00-0.00	60
6	LSEIK-2 versus LSEIK-1	1-1-1	0.04-0.00-0.00	182
7	Forecast initialized on 21 Nov 2011 versus LSEIK-1	1-1-1	0.00-0.00-0.00	182
8	Forecast initialized on 1 Dec 2011 versus LSEIK-1	0-0-1	0.37-0.81-0.00	122
9	Forecast initialized on 1 Jan 2012 versus LSEIK-1	0-0-1	0.77-0.94-0.00	61
10	Forecast initialized on 1 Nov 2011 versus LSEIK-2	1-1-1	0.00-0.00-0.00	182
11	Forecast initialized on 1 Dec 2011 versus LSEIK-2	1-1-1	0.00-0.00-0.00	122
12	Forecast initialized on 1 Jan 2012 versus LSEIK-2	0-1-1	0.12-0.02-0.00	61

[a]For example, LSEIK-2 versus LSEIK-1 means that the RMSE of LSEIK-2 relative to data (SSMIS, OSISAF, SMOS) is compared to the RMSE of LSEIK-1 to the same data, with the null hypothesis that they are the same. The *t* test2 flag is set to 1 for rejecting and 0 for not rejecting the null hypothesis. The triple of values refer to the three different data sets SSMIS-OSISAF-SMOS.

The sea ice thickness observational errors σ_{SIT} in the data assimilation system were initially approximated by a constant value. A calibration of the value did not allow us to get any reasonable forecast of the sea ice conditions. A consideration of various ranges of relative errors depending on the ice thickness, however, leads to an improved situation (not shown). The best results presented here were obtained with the sea ice thickness data errors explicitly prescribed by available observational uncertainty estimates [*Tian-Kunze et al.*, 2014]. No additional out weighting—neither model, nor data—was required.

6. Results

To assess the data assimilative system's performance, we focus on the system's forecasting skill and consider sea ice forecasts for 24 h, 1, 2, and 3 months initialized with a model state corrected after the filter analysis. After initialization, the 1–3 months simulations are not corrected by data assimilation again, while the 24 h simulations are updated every day. As a measure of the forecasting skill improvement, we consider a decrease of mean and root mean squared estimates of the forecast deviation from available observation in comparison with model performance without any data assimilation. The experiments with forecasts over the periods of 1, 2, and 3 months are shown in the context of evaluating possible prediction periods subject to existing model bias due to uncertainties in internal parameterizations and discrepancies in external forcing.

Table 1 summarizes two-sample *t* test (*t* test2) statistics that describe to what extent the differences between two data sets are significant. The null hypothesis that the two data series (here: RMSE time series) are independent random samples from normal distributions with equal means and equal but unknown variances is rejected at a specific significance level (0.05 in our case) when the *t* test2 returns 1. Zero means that, based on the *t* test2, the null hypothesis cannot be rejected.

6.1. Sea Ice Concentration Forecast
Figure 2 compares the temporal evolution of the root mean square error (RMSE) of the ice concentration forecast with respect to the assimilated NSIDC SSMIS (Figure 2a) and the OSISAF data (Figure 2b) over the period of 1 November 2011 to 31 January 2012. To avoid large errors in small concentrations and to be consistent with *Lisæter et al.* [2003] and *Yang et al.* [2014], all RMSEs were taken only over the grid points where either the model or the observations have ice concentrations larger than 0.05.

In both experiments with data assimilation, the deviation of all predicted sea ice concentrations from the assimilated SSMIS concentration and the independent OSISAF data was significantly reduced (see Figure 2 and the two-sample *t* test results in rows 1 and 2 of Table 1). For most of the time, the LSEIK-2 results are only slightly closer to the satellite observations than the LSEIK-1 concentrations, but this difference is significant at the 0.95 confidence level (row 6 in Table 1). The total RMSE (RMSE over all points in space and time) of the run without data assimilation, the LSEIK-1 and LSEIK-2 24 h forecasts with respect to the assimilated SSMIS data are 0.16, 0.13, and 0.12. Both the improvements of LSEIK-1 and LSEIK-2 over MITgcm without
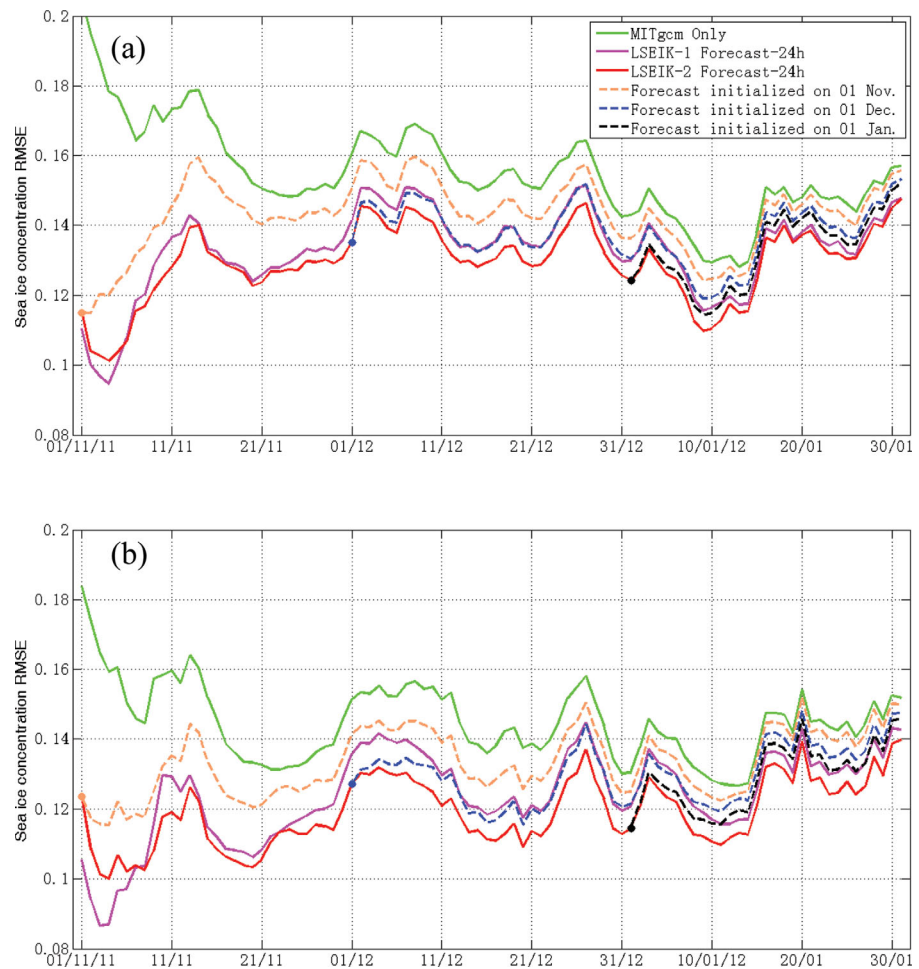
Figure 2. Temporal evolution of RMSE differences between (a) NSIDC SSMIS/(b) OSIAF ice concentration data and MITgcm forecast (green solid), LSEIK-1 24 h forecast (magenta solid), LSEIK-2 24 h forecast (red solid) over the period 1 November 2011 to 31 January 2012. The 1, 2, and 3 month(s) forecasts with LSEIK-2 intialization on 1 November 2011, 1 December 2011, and on 1 January 2012 are also shown as copper, blue, and black dashed lines.

data assimilation tend to decrease over the period and show that the LSEIK filtering effects on the ice concentration are weaker in winter (December-February) than in autumn (September-November). In contrast, the corresponding LSEIK-1 experiment in *Yang et al*. [2014] showed a strong effect of assimilating ice concentration data in summer (June-August). In winter, however, rapid ice growth leads to ice concentrations of 1 (100%) in the central Arctic Ocean in all model ensemble members, so that the ensemble variability decreases and consequently the correlations between ice concentrations and thicknesses become weaker [see also *Lisæter et al*., 2003]. The ice concentration forecast from LSEIK-2 with SMOS ice thickness data is similar to the LSEIK-1 forecast. The impact of the additional data is small because SMOS grid points with ice thickness below 1.0 m are limited in winter (purple dotted line in Figure 3 shows the fraction valid SMOS thickness data points to all SMOS grid points).

The long-term concentration forecasts initialized in the beginning of each month (copper, blue, and black lines) have lower RMSEs with respect to the assimilated sea ice concentration data (Figure 2a) compared to the model simulations without assimilation. As the impact of the data assimilation decreased over the season because of the closing ice cover, the forecast skill (improvement over MITgcm without DA) also decreased. As shown in row 12 of Table 1, there is a probability of 12% that they are the same, that is, the 1 month forecast does not significantly differ from the series of 24 h forecasts (row 12 in Table 1). The 3 months forecast initialized on 1 November 2011 agrees significantly better with the now independent concentration data than the model simulation without data assimilation (row 3 in Table 1) and still has improved skill at the end of the simulation period. The RMSEs of the 2 months forecast (blue line) that starts
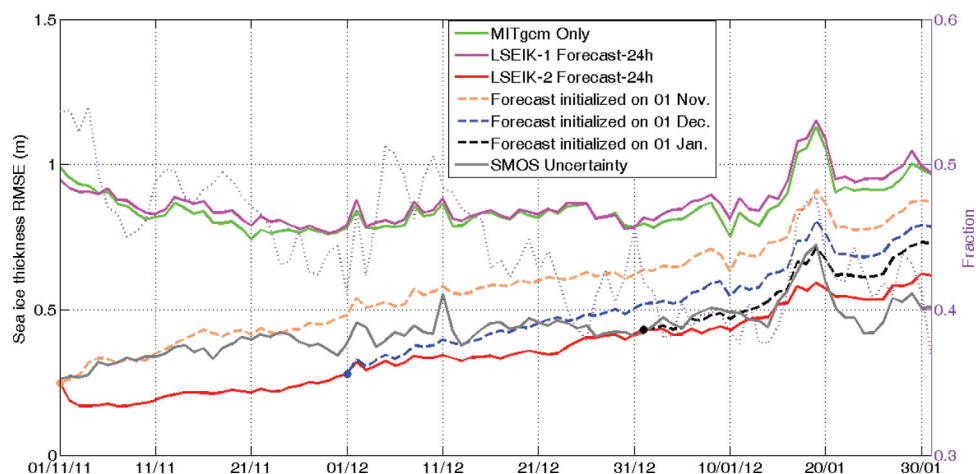
Figure 3. Temporal evolution of RMSE differences between SMOS ice thickness (<1.0 m) and MITgcm forecast (green solid), LSEIK-1 24 h forecast (magenta solid), LSEIK-2 24 h forecast (red solid) over the period 1 November 2011 to 31 January 2012. The 1, 2, and 3 month(s) forecasts with LSEIK-2 intialization on 1 November 2011, 1 December 2011, and 1 January 2012 are also shown as copper, blue, and black dashed lines. The mean uncertainties of SMOS ice thickness (<1.0 m) are shown in gray solid line. The fractions of 0–1 m SMOS thickness in the total SMOS ice area are shown in purple dotted lines (corresponding to the right-hand side axes).

after the first month of daily analyses are close to the series of daily updated forecasts with sea ice concentration assimilation (LSEIK-1, magenta line). This is consistent with the p values of 0.37 in row 8 of Table 1, which shows the null hypothesis test cannot by rejected at the 0.05 significance level, and the RMSEs with the assimilated NSIDC ice concentration observations are the same with a high probability of 37%.

6.2. Sea Ice Thickness Forecast

Figure 3 compares the temporal evolution of the RMSE of the ice thickness forecast with respect to the assimilated SMOS ice thickness (<1.0 m) over the period of 1 November 2011 to 31 January 2012. For the entire period, the hypothesis test suggests at the 0.05 significance level that the LSEIK-1 forecast is not different from the free MITgcm run (row 1 in Table 1). Again in contrast, the impact of assimilating ice concentration on thickness fields was larger in summer [*Yang et al.*, 2014]. When assimilating the SMOS sea ice thickness, the agreement between LSEIK-2 predicted thickness and SMOS data is significantly better (row 2 in Table 1). The total RMSE of the run without data assimilation, the LSEIK-1, and LSEIK-2 24 h forecasts are 0.85, 0.87, and 0.38 m. But as for the ice concentration forecast, this improvement in LSEIK-2 also decreases from November to January. In order to explain this behavior, we invoke the same argument of a gradually decreasing number of ice thickness grid points (<1.0 m) during the freezing conditions that can be used in the LSEIK-2 analysis, the fraction of used grid points in the total SMOS sea ice grid points varies between 0.54 and 0.37 with a decreasing trend (purple dotted line in Figure 3).

The long-term thickness forecasts starting each month (copper, blue, and black lines) have a remarkably reduced RMSE with respect to the assimilated sea ice thickness data compared to the model simulations without assimilation (rows 3–5 in Table 1) or only ice concentration assimilation (rows 7–9 in Table 1). The 1 month forecast, despite being less accurate than the 24 h forecast, is still significantly closer to the observations in comparison with the forecast without any data assimilation. The 2 and 3 months forecasts also remained closer to the thickness satellite data and still had improved skill at the end of the simulation period, even though the forecasting skill decreased in comparison with the forecast based on data assimilation every 24 h. The last circumstance, however, shows that the model system possesses some bias and still can be optimized by adjusting internal parameters or parameterizations and assessing the forcing.

In Figure 4, we show the maps of the mean ice thickness differences between the unassimilated run and LSEIK-1 and LSEIK-2. In LSEIK-1, the assimilation impacts are generally small and most of the changes are in the marginal ice zone (Figure 4a). In LSEIK-2, the strongly overestimated sea ice thickness in the model without data assimilation is reduced and hence corrected toward the SMOS observations (right panel), especially in the thin first year ice areas surrounding the central Arctic. The change of multiyear ice thickness in the interior Arctic is small because most assimilated thin SMOS ice thickness (<1.0 m) is observed outside the
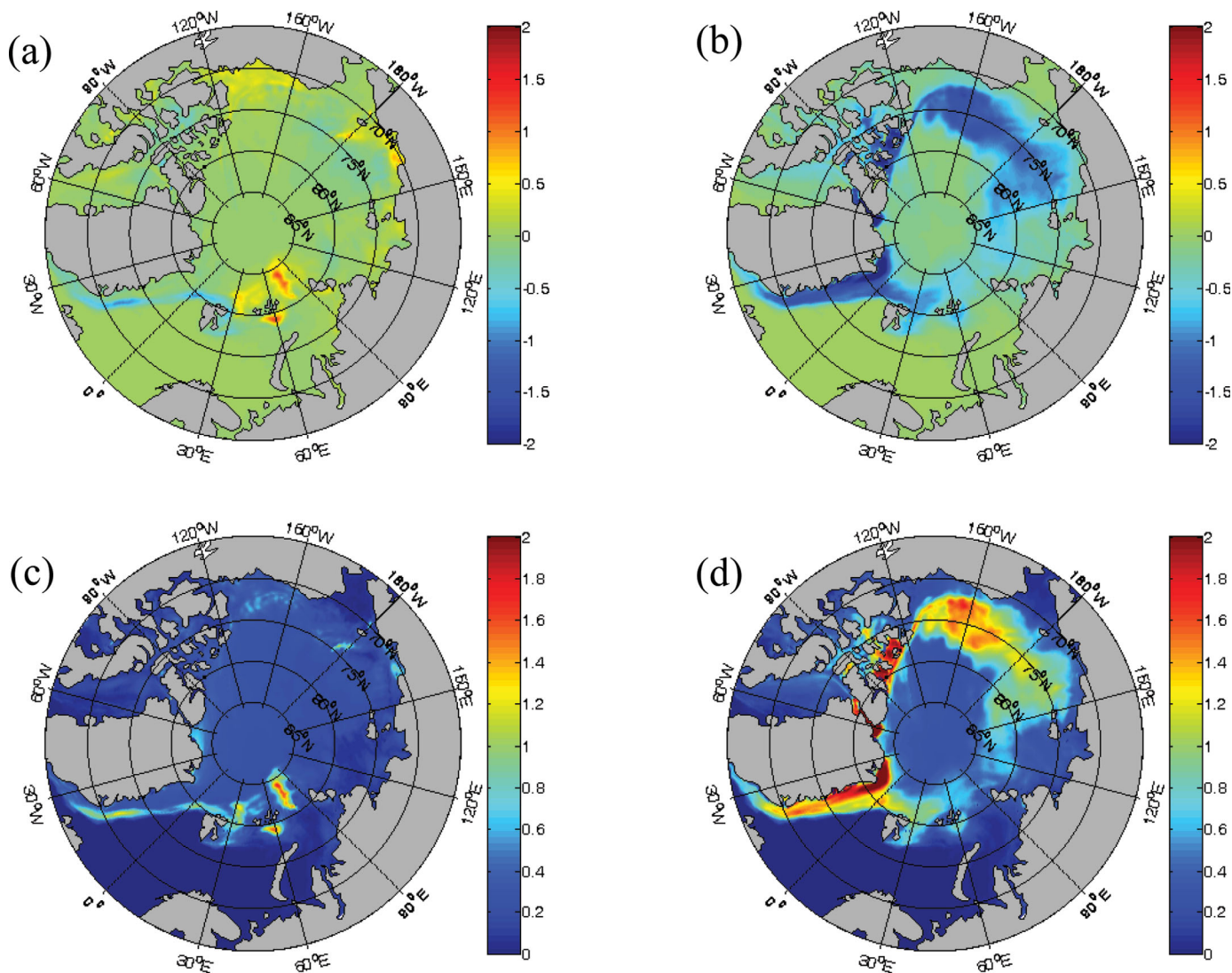
Figure 4. (a and b) Mean deviation and (c and d) RMSE deviation of the LSEIK-1 (Figures 4a and 4c) and LSEIK-2 (Figures 4b and 4d) sea ice thickness 24 h forecast from the MITgcm forecast without assimilation averaged over the period 1 November 2011 to 31 January 2012.

central Arctic. Still there is some influence in this area despite the unavailability of data for assimilation. As seen from the histograms of LSEIK-2 ice thickness forecast improvement over MITgcm forecast without DA on 5 November 2011, most of the thicknesses have been reduced in the SMOS 0–1 m thickness (Figure 5b) range. During the analysis phase, most of the thickness updates (LSEIK-2 analysis-LSEIK-2 forecast) are within a few centimeters, and the fraction of grid points with a reduced thickness is about 80% (Figure 5d).

6.3. Comparison With Independent Data

Comparing the three ice thickness solutions with and without assimilation against BGEP_2011a, BGEP_2011b, BGEP_2011d observations (Figure 6) suggests again that assimilation of ice thickness significantly improves the simulated sea ice thickness. All three forecasts reproduce the gradually increasing ice thickness at BGEP_2011a, BGEP_2011b, BGEP_2011d, but without assimilating ice thickness data, the model bias is large (∼2m) compared to the observations. The hypothesis tests show that with the SSMIS ice concentration assimilation in LSEIK-1, this ice thickness bias has not been reduced, but the assimilation of SMOS ice thickness in LSEIK-2 reduced most of the thickness bias. The mean thickness deviation at BGEP_2011a, BGEP_2011b, and BGEP_2011d have been changed from 1.61 ± 0.23, 1.45 ± 0.28, and 1.34 ± 0.38 m in case of the run without assimilation (row 1, 6, and 11 in Table 2) to 0.31 ± 0.25, 0.92 ± 0.57, and 0.17 ± 0.28 m in LSEIK-2 (row 3, 8, and 13 in Table 2). The improvements at BGEP_2011b (magenta
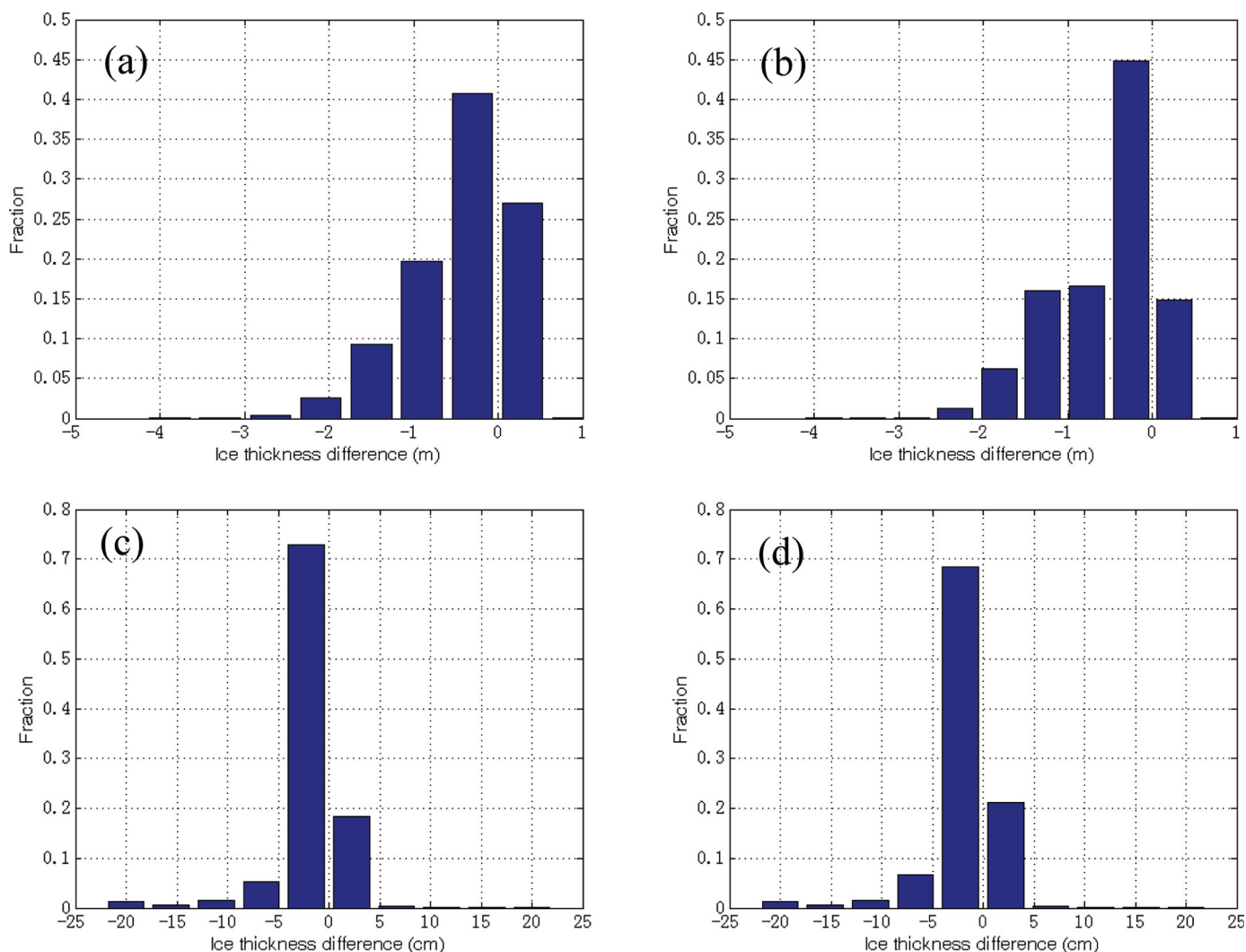
Figure 5. Histograms of sea ice thickness difference between LSEIK-2 forecast and MITgcm forecast without (a and b) DA (LSEIK-2 forecast-MITgcm), and (c and d) thickness update (LSEIK-2 analysis-LSEIK-2 forecast) on 5 November 2010, over the total sea ice area (Figure 5a and 5c) and the 0–1 m SMOS thickness area (Figures 5b and 5d).

square in Figure 1) are smaller than at BGEP_2011a and BGEP_2011d, because BGEP_2011b is closer to the central Arctic (∼78°N) than the other two ULS devices (Figure 1). In the central Arctic there is thicker ice and hence in winter there are not enough SMOS observations that can be used in the assimilation (purple dotted line in Figure 6b).

As for the ULS data, all three solutions captured the increasing ice thickness found in the IMB_2011K data. The LSEIK-1 forecast with sea ice concentration data assimilation slightly reduced the thickness bias compared to the MITgcm simulation without data assimilation, the mean thickness deviation has been changed from 1.73 ± 0.16 m in the case of the run without assimilation (row 16 in Table 2) to 1.64 ± 0.15 m in LSEIK-1 (row 17 in Table 2). The LSEIK-2 simulation with SMOS ice thickness assimilation agrees best with the IMB observations over the entire period with a reduced RMSE of 0.42 m (row 18 in Table 2).

7. Summary and Conclusions

A localized Singular Evolutive Interpolated Kalman (LSEIK) filter has been implemented in a coupled sea ice-ocean model to assimilate the first continuous satellite-based near real-time sea ice thickness operational data—the SMOS sea ice thickness. NSIDC SSMIS sea ice concentration data were also assimilated in the period of 1 November 2011 to 31 January 2012. The experiments show that the assimilation of SMOS ice thickness reduces the model bias with respect to both observed sea ice thickness and concentration.
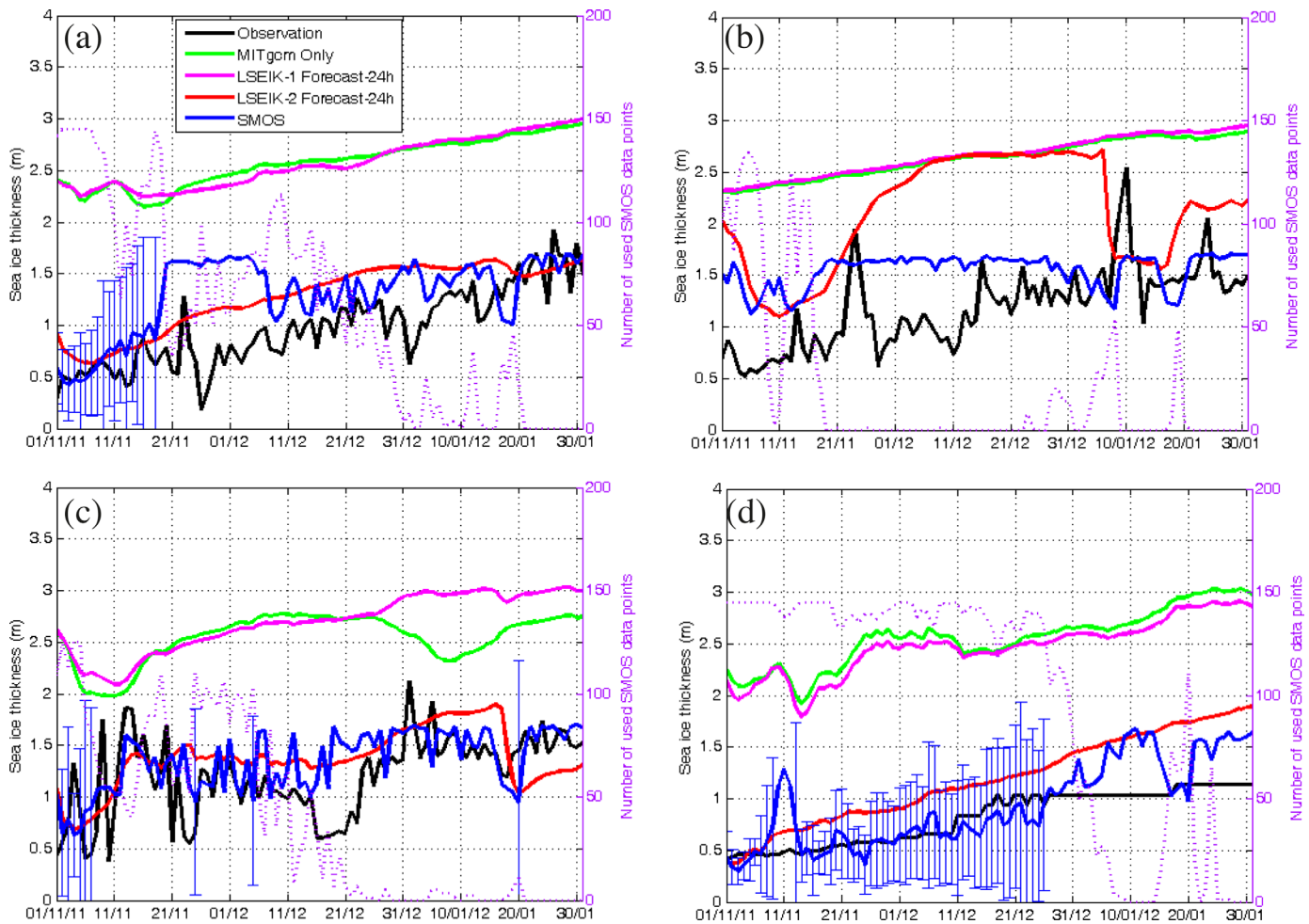
Figure 6. Sea ice thickness evolution at (a) BGEP_2011a, (b) BGEP_2011b, (c) BGEP_2011d, (d) IMB_2011K from 1 November 2011 to 31 January 2012: observation (black curve), MITgcm forecast without assimilation (green curve), LSEIK-1 24 h forecast (magenta curve), LSEIK-2 24 h forecast (red curve), interpolated thickness from all the SOMS data (blue curve), and interpolated uncertainties from the uncertainties of 0–1 m SMOS data (blue bars). The number of 0–1 m SMOS data values in the radius of seven model grid points (∼126 km) are shown in purple dotted lines.

Further, the assimilation of observed SMOS sea ice thickness improves the ice thickness forecasts compared to the model forecasts with ice concentration assimilation only or without any data assimilation, and the improvement is mainly in the first-year ice zone.

The most striking result is related to the thickness forecasts with SMOS ice thickness assimilation. These forecasts have remarkably reduced systematic errors over the forecasts with ice concentration assimilation only or without any data assimilation and the total RMSE has been reduced from 0.85 to 0.38 m. This result suggests that the corrections in the mean state of the sea ice concentration and thickness creates a system memory that allows for forecasts with some skill over long periods. The impact of the assimilation changes over the 3 months period. The RMSE time series of all forecasts tend to converge toward the end of January 2012, because by that time most of the Arctic is 100% ice covered so that concentration data does not add any information. Further, the ice cover is mostly thick (>1m) and hence outside the thickness range for which SMOS data are accurate enough to be used for data assimilation.

Assimilation of summer sea ice concentration with a LSEIK filter in a coupled ice-ocean model was recently discussed [*Yang et al.*, 2014]. It was shown how the concentration data provide improved estimates of summer sea ice concentration estimates. Further, the summer sea ice thickness could also be improved, most likely due to the multivariate covariance between ice concentration and thickness that was used in the LSEIK filter. Now we find, however, that this improvement is small in the cold season when the covariance between ice concentration and ice thickness is weak when the ice concentration tends toward

Table 2. Mean, Standard Deviation (STD), and RMSE of the Differences Between Ice Thickness Estimates

		Statistics	Mean (m)	STD (m)	RMSE (m)
BGEP_2011a	1	MITgcm versus observation	1.61	0.23	1.62
	2	LSEIK-1 versus observation	1.60	0.21	1.61
	3	LSEIK-2 versus observation	0.31	0.25	0.39
	4	SMOS versus observation	0.33	0.38	0.50
	5	LSEIK-2 versus LSEIK-1	−1.29	0.17	1.30
BGEP_2011b	6	MITgcm versus observation	1.45	0.28	1.48
	7	LSEIK-1 versus observation	1.48	0.28	1.50
	8	LSEIK-2 versus observation	0.92	0.57	1.08
	9	SMOS versus observation	0.37	0.38	0.52
	10	LSEIK-2 versus LSEIK-1	−0.56	0.48	0.73
BGEP_2011d	11	MITgcm versus observation	1.34	0.38	1.41
	12	LSEIK-1 versus observation	1.49	0.38	1.54
	13	LSEIK-2 versus observation	0.17	0.28	0.41
	14	SMOS versus observation	0.15	0.35	0.38
	15	LSEIK-2 versus LSEIK-1	−1.32	0.26	1.35
IMB_2011K	16	MITgcm versus observation	1.73	0.16	1.74
	17	LSEIK-1 versus observation	1.64	0.15	1.65
	18	LSEIK-2 versus observation	0.36	0.20	0.42
	19	SMOS versus observation	0.12	0.26	0.28
	20	LSEIK-2 versus LSEIK-1	−1.27	0.21	1.29

uniform values of 100% in the Arctic Ocean. The SMOS sea ice thickness therefore provide valuable additional information to provide improved thickness forecasts with assimilated sea ice models.

This study represents an additional step of the work described in *Yang et al.* [2014] toward an Arctic sea ice-ocean forecast system. Although SMOS ice thickness data are limited to the cold season and not applicable during summer, the experiments in this study show how sea ice forecasts can improve by assimilating ice thickness measurements. We conclude that such an Arctic sea ice-ocean forecast system has the potential for further optimization and extension by assimilating additional sea ice-ocean data sets, for example, ice velocity, sea surface temperature, and sea surface level anomaly.

References

Cavalieri, D. J., C. L. Parkinson, N. DiGirolamo, and A. Ivanoff (2012), Intersensor calibration between F13 SSMI and F17 SSMIS for global sea ice data records, *IEEE Trans. Geosci. Remote Sens.*, *9*(2), 233–236.

Eastwood, S., K. R. Larsen, T. Lavergne, E. Neilsen, and R. Tonboe (2011), OSI SAF global sea ice concentration reprocessing: Product user manual, Version 1.3, report, SAF/OSI/CDOP/met.no/TEC/MA/138.

Eicken, H. (2013), Ocean science: Arctic sea ice needs better forecasts, *Nature*, *497*(7450), 431–433.

Gaspari, G., and S. E. Cohn (1999), Construction of correlation functions in two and three dimensions, *Q. J. R. Meteorol. Soc.*, *125*(554), 723–757.

Huntemann, M., G. Heygster, L. Kaleschke, T. Krumpen, M. Mäkynen, and M. Drusch (2014), Empirical sea ice thickness retrieval during the freeze up period from SMOS high incident angle observations, *Cryosphere*, *8*(2), 439–451, doi:10.5194/tc-8-439-2014.

Janjić, T., L. Nerger, A. Albertella, J. Schröter, and S. Skachko (2011), On domain localization in ensemble based Kalman filter algorithms, *Mon. Weather Rev.*, *139*, 2046–2060.

Kaleschke, L., N. Maaß, C. Haas, S. Heygster, and R. Tonboe (2010), A sea-ice thickness retrieval model for 1.4 GHz radiometry and application to airborne measurements over low salinity sea-ice, *Cryosphere*, *4*, 583–592, doi:10.5194/tc-4-583-2010.

Kaleschke, L., X. Tian-Kunze, N. Maaß, M. Mäkynen, and M. Drusch (2012), Sea ice thickness retrieval from SMOS brightness temperatures during the Arctic freeze-up period, *Geophys. Res. Lett.*, *39*, L05501, doi:10.1029/2012GL050916.

Kivman, G. A., A. L. Kurapov, and A. Guessen (2001), An entropy approach to tuning weights and smoothing in the generalized inversion, *J. Atmos. Oceanic Technol.*, *18*, 266–276.

Kwok, R., and D. Rothrock (2009), Decline in Arctic sea ice thickness from submarine and ICESat records: 1958–2008, *Geophys. Res. Lett.*, *36*, L15501, doi:10.1029/2009GL039035.

Kwok, R., and D. Sulsky (2010), Arctic Ocean sea ice thickness and kinematics: Satellite retrievals and modeling, *Oceanography*, *23*(4), 134–143.

Lindsay, R. W., and J. Zhang (2006), Assimilation of ice concentration in an ice-ocean model, *J. Atmos. Oceanic Technol.*, *23*(5), 742–749.

Lisæter, K., G. Evensen, and S. Laxon (2007), Assimilating synthetic CryoSat sea ice thickness in a coupled ice-ocean model, *J. Geophys. Res.*, *112*, C07023, doi:10.1029/2006JC003786.

Lisæter, K. A., J. Rosanova, and G. Evensen (2003), Assimilation of ice concentration in a coupled ice–ocean model, using the Ensemble Kalman filter, *Ocean Dyn.*, *53*(4), 368–388.

Losa, S. N., S. Danilov, J. Schröter, L. Nerger, S. Maβmann, and F. Janssen (2012), Assimilating NOAA SST data into the BSH operational circulation model for the North and Baltic Seas: Inference about the data, *J. Mar. Syst.*, *105*, 152–162.

Losa, S. N., S. Danilov, J. Schröter, T. Janjić, L. Nerger, and F. Janssen (2014), Assimilating NOAA SST data into BSH operational circulation model for the North and Baltic Seas: Part 2. Sensitivity of the forecast's skill to the prior model error statistics, *J. Mar. Syst.*, *129*, 259–270.

Losch, M., D. Menemenlis, J.-M. Campin, P. Heimbach, and C. Hill (2010), On the formulation of sea ice models. Part 1: Effects of different solver implementations and parameterizations, *Ocean Modell.*, *33*(1), 129–144.

Marshall, J., A. Adcroft, C. Hill, L. Perelman, and C. Heisey (1997), A finite-volume, incompressible Navier Stokes model for studies of the ocean on parallel computers, *J. Geophys. Res.*, *102*(C3), 5753–5766.

Mecklenburg, S., M. Drusch, Y. H. Kerr, J. Font, M. Martin-Neira, S. Delwart, G. Buenadicha, N. Reul, E. Daganzo-Eusebio, and R. Oliva (2012), ESA's soil moisture and ocean salinity mission: Mission performance and operations, *IEEE Trans. Geosci. Remote Sens.*, *50*(5), 1354–1366.

Melling, H., P. H. Johnston, and D. A. Riedel (1995), Measurements of the underside topography of sea ice by moored subsea sonar, *J. Atmos. Oceanic Technol.*, *12*(3), 589–602.

Menemenlis, D., J.-M. Campin, P. Heimbach, C. Hill, T. Lee, A. Nguyen, M. Schodlok, and H. Zhang (2008), ECCO2: High resolution global ocean and sea ice data synthesis, *Mercator Ocean Q. Newsl.*, *31*, 13–21.

Nerger, L., and W. Hiller (2013), Software for ensemble-based data assimilation systems—Implementation strategies and scalability, *Comput. Geosci.*, *55*, 110–118.

Nerger, L., S. Danilov, W. Hiller, and J. Schröter (2006), Using sea-level data to constrain a finite-element primitive-equation ocean model with a local SEIK filter, *Ocean Dyn.*, *56*(5-6), 634–649.

Nguyen, A. T., D. Menemenlis, and R. Kwok (2011), Arctic ice-ocean simulation with optimized model parameters: Approach and assessment, *J. Geophys. Res.*, *116*, C04025, doi:10.1029/2010JC006573.

Nguyen, A. T., R. Kwok, and D. Menemenlis (2012), Source and pathway of the Western Arctic upper halocline in a data-constrained coupled ocean and sea ice model, *J. Phys. Oceanogr.*, *42*(5), 802–823.

Onogi, K., J. Tsutsui, H. Koide, M. Sakamoto, S. Kobayashi, H. Hatsushika, T. Matsumoto, N. Yamazaki, H. Kamahori, and K. Takahashi (2007), The JRA-25 reanalysis, *J. Meteorol. Soc. Jpn.*, *85*(3), 369–432.

Perovich, D. K., J. A. Richter-Menge, B. Elder, K. Claffey, and C. Polashenski (2009), Observing and understanding climate change: Monitoring the mass balance, motion, and thickness of Arctic sea ice. [Available at http://imb.crrel.usace.army.mil/.]

Pham, D. T. (2001), Stochastic methods for sequential data assimilation in strongly nonlinear systems, *Mon. Weather Rev.*, *129*(5), 1194–1207.

Richter-Menge, J. A., D. K. Perovich, B. C. Elder, K. Claffey, I. Rigor, and M. Ortmeyer (2006), Ice mass-balance buoys: A tool for measuring and attributing changes in the thickness of the Arctic sea ice cover, *Ann. Glaciol.*, *44*(1), 205–210.

Rollenhagen, K., R. Timmermann, T. Janjić, J. Schröter, and S. Danilov (2009), Assimilation of sea ice motion in a finite-element sea ice model, *J. Geophys. Res.*, *114*, C05007, doi:10.1029/2008JC005067.

Schweiger, A., R. Lindsay, J. Zhang, M. Steele, H. Stern, and R. Kwok (2011), Uncertainty in modeled Arctic sea ice volume, *J. Geophys. Res.*, *116*, C00D06, doi:10.1029/2011JC007084.

Smith, W. H., and D. T. Sandwell (1997), Global sea floor topography from satellite altimetry and ship depth soundings, *Science*, *277*(5334), 1956–1962.

Stark, J., J. Ridley, M. Martin, and A. Hines (2008), Sea ice concentration and motion assimilation in a sea ice−ocean model, *J. Geophys. Res.*, *113*, C05S91, doi:10.1029/2007JC004224.

Stroeve, J. C., M. C. Serreze, M. M. Holland, J. E. Kay, J. Malanik, and A. P. Barrett (2012), The Arctic's rapidly shrinking sea ice cover: A research synthesis, *Clim. Change*, *110*(3-4), 1005–1027.

Tian-Kunze, X., L. Kaleschke, N. Maaß, M. Mäkynen, N. Serra, M. Drusch, and T. Krumpen (2014), SMOS-derived thin sea ice thickness: Algorithm baseline, product specifications and initial verification, *Cryosphere*, *8*, 997–1018, doi:10.5194/tc-8-997-2014.

Tietsche, S., D. Notz, J. Jungclaus, and J. Marotzke (2013), Assimilation of sea ice concentration in a global climate model- physical and statistical aspects, *Ocean Sci.*, *9*(1), 19–36.

Tonboe, R., and E. Nielsen (2010), Global sea ice concentration reprocessing validation report, Product OSI-409, Version 1, report, SAF/OSI/CDOP/met.no/TEC/RP/150.

Yang, Q., N. S. Losa, M. Losch, J. Liu, Z. Zhang, L. Nerger, and H. Yang (2014), Assimilating summer sea ice concentration into a coupled ice-ocean model using a localized SEIK filter, *Ann. Glaciol.*, *56*(69), 38–44, doi:10.3189/2015AoG69A740.

Zhang, J., and W. Hibler III (1997), On an efficient numerical method for modeling sea ice dynamics, *J. Geophys. Res.*, *102*(C4), 8691–8702.